Vol 18 No 8, August 2009
1674-1056/2009/18(08)/3422-09

Chinese Physics B

© 2009 Chin. Phys. Soc.
and IOP Publishing Ltd

Electromagnetic scattering from two-layer rough interfaces in the Kirchhoff approximation*

Wang Rui(王 蕊)†, Guo Li-Xin(郭立新), and Ma Jun(麻 军)

School of Science, Xidian University, Xi'an 710071, *China*

(Received 12 May 2008; revised manuscript received 10 November 2008)

Electromagnetic wave scattering from multilayers consisting of two two-layer Gaussian rough surfaces with lossless media is investigated in the Kirchhoff approximation (KA), with consideration of the shadowing effects. The tapered incident wave is introduced into the classic KA, and the bistatic scattering coefficient is redetermined. The advantage of this method is that it is faster in computation than the exact numerical methods. The numerical results show that the bistatic scattering coefficient calculated in the KA is in good agreement with that obtained by using the method of moment (MOM) over a most angular range, which indicates the validity of the KA proposed in our paper. Finally, the effects of the relative permittivity, the root-mean-square (RMS) height, the correlative length, and the average height between the two interfaces on the bistatic scattering coefficient are discussed in detail.

Keywords: two-layer Gaussian rough surface, Kirchhoff approximation, tapered wave
PACC: 4110H, 4120

1. Introduction

Electromagnetic wave scattering from layered rough surfacs has been intensively investigated for its applications in a number of important research areas,[1−5] such as remote sensing, ocean engineering etc. Remote sensing can be used for detecting and monitoring possible oil spills on ocean surfaces. However, other phenomena may lead to the same effects on measurements. In order to ascertain such an environmental effect on measurements, we focus on the issues of wave scattering from rough surfaces in microwave and optical ranges. Electromagnetic models for rough surface scattering have been developed for several years; however, in these models only a single layer is generally considered, that is to say, one rough interface. Their extension to multilayer separated by rough interfaces has been studied analytically.[6] In the present paper the tapered incident wave, which is commonly used in the MOM for calculating rough surface scattering, is introduced into the classical KA and the bistatic scattering coefficient is redetermined to calculate the scattering from the multilayer consisting of two one-dimensional rough surfaces. Also the influence of the shadowing effect[7,8] is taken into account in the KA so as to make the results more accurate.

The remainder of the present paper is organized as follows. The scattering model is developed in Section 2. The theoretical formulation of the KA and the redetermination of bistatic scattering coefficient with consideration of the shadowing effects are developed in Section 3. Then the numerical results on the scattering coefficient of the two-layer model are given and discussed in Section 4. Finally given in Section 5 are the conclusions and further investigation in this topic.

2. The scattering model

As depicted in Fig.1, the considered multilayer configuration consists of two one-dimensional Gaussian rough interfaces: one is the upper interface S_0, which separates a lossless homogeneous dielectric medium $\Omega_0(\varepsilon_0, \mu_0)$ with relative permittivity $\varepsilon_0 = 1$ and permeability $\mu_0 = 1$, from a lossless medium $\Omega_1(\varepsilon_1, \mu_1 = \mu_0)$, and the other is lower interface S_1, which separates the homogeneous medium Ω_1 that is filled between interfaces S_0 and S_1, from the semi-infinite lower medium $\Omega_2(\varepsilon_2, \mu_2 = \mu_0)$. Each boundary is invariant with respect to any translation along

*Project supported by the National Natural Science Foundation of China (Grant No 60571058), and the Specialized Research Fund for the Doctoral Program of Higher Education, China (Grant No 20070701010).
†Corresponding author. E-mail: doufuruier@yahoo.cn

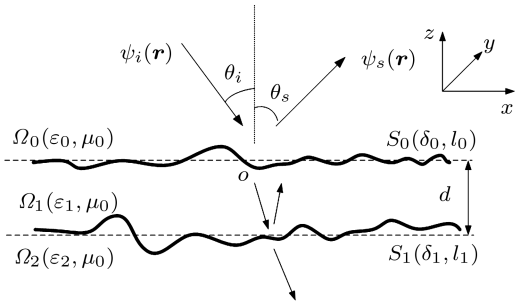


Fig.1. Geometric model of two-layer Gaussian rough surfaces.

the y axis. The height profiles of surfaces S_0 and S_1 are given by $z_0 = f_0(x)$ and $z_1 = f_1(x)$ respectively. d is the average height between the two Gaussian rough interfaces.

For the scattering computation, the two-layer surface realizations are needed at a set of P points with spacing Δx over length $L = P\Delta x$. Realizations with the desired properties can be generated at points $x_p = p\Delta x$ $(p = 1, \ldots, P)$ using

$$f_{0,1}(x_p) = \frac{1}{L}\sum_{i=-P/2}^{P/2-1} F(K_i)\exp(jK_i x_p), \tag{1}$$

where, for $i \geq 0$,

$$F(K_i) = \sqrt{2\pi LW(K_i)}\begin{cases}[N(0,1) + jN(0,1)]/\sqrt{2}, & i \neq 0, P/2,\\ N(0,1), & i = 0, P/2,\end{cases} \tag{2}$$

and for $i < 0$, $F(K_i) = F(K_{-i})^*$. $K_i = 2\pi i/L$ and each time $N(0,1)$ appears, which indicates an independent sample taken from a zero mean, unit variance Gaussian distribution. For the present work, the rough surface model used in the scattering model is generated randomly with a Gaussian roughness spectrum, i.e.[9]

$$W(K_i) = (l_{0,1}\delta_{0,1}^2/2\sqrt{\pi})\mathrm{e}^{-K_i^2 l_{0,1}^2/4}, \tag{3}$$

where $\delta_{0,1}$ and $l_{0,1}$ denote the root-mean-square (RMS) heights and the correlation lengths of the upper and the lower surfaces, respectively. Expression (1) is computed by using a fast Fourier transform (FFT). We can choose different values of the parameters ($\delta_{0,1}$, $l_{0,1}$) for upper and the lower Gaussian rough surfaces.

3. Theoretical formulation of Kirchhoff approximation

Consider a wave $\psi_i(\boldsymbol{r})$ $(\boldsymbol{r} = x\hat{x} + z\hat{\boldsymbol{z}})$ impinging on a random two-layer Gaussian rough surface (Fig.1) with the correlation lengths l_0 and l_1 and the RMS heights δ_0 and δ_1, respectively. The total field $\psi(\boldsymbol{r})$ in medium Ω_0 is

$$\psi(\boldsymbol{r}) = \psi_i(\boldsymbol{r}) + \psi_s(\boldsymbol{r}), \tag{4}$$

where $\psi_s(\boldsymbol{r})$ is the scattered field, which consists of the scattered field ψ_{00}^{sc} from the upper surface due to the incident field in medium Ω_0 and the transmitted field ψ_{10}^{tr} from medium Ω_1. It should be noted that the ψ_i may be defined as $\boldsymbol{E}_i(\boldsymbol{r}) = \psi_i(\boldsymbol{r})\hat{\boldsymbol{y}}$ for horizontal polarization and $\boldsymbol{H}_i(\boldsymbol{r}) = \psi_i(\boldsymbol{r})\hat{\boldsymbol{y}}$ for vertical polarization.

We can write an analytical expression of the scattered field $\psi_s(\boldsymbol{r})$ in medium Ω_0. The scattered field due to the rough upper and the rough lower interfaces is obtained by using the Huygens's principle:[10]

$$\psi_s(\boldsymbol{r}) = \int_{S_0}\left[\psi(\boldsymbol{r}_0)\frac{\partial G(\boldsymbol{r},\boldsymbol{r}_0)}{\partial n_0} - G(\boldsymbol{r},\boldsymbol{r}_0)\frac{\partial\psi(\boldsymbol{r}_0)}{\partial n_0}\right]\mathrm{d}S_0, \tag{5}$$

where $\psi(\boldsymbol{r}_0)$ denotes the total field of $\boldsymbol{r}_0$ in surface S_0, G is two-dimensional Green's function in the free space

$$G(\boldsymbol{r},\boldsymbol{r}_0) = \frac{\mathrm{i}}{4}H_0^{(1)}(k\,|\boldsymbol{r}-\boldsymbol{r}_0|), \tag{6}$$

and the normal derivative of the Green's function[11]

$$\frac{\partial G(\boldsymbol{r},\boldsymbol{r}_0)}{\partial n_0} = \frac{\mathrm{i}k}{4}\hat{\boldsymbol{n}}_0\cdot\frac{\boldsymbol{r}-\boldsymbol{r}_0}{|\boldsymbol{r}-\boldsymbol{r}_0|}H_1^{(1)}(k\,|\boldsymbol{r}-\boldsymbol{r}_0|). \tag{7}$$

Here $\hat{\boldsymbol{n}}_0$ is the unit normal vector of the rough surface S_0

$$\hat{\boldsymbol{n}}_0 = \frac{-f_0'(x)\hat{\boldsymbol{x}} + \hat{\boldsymbol{z}}}{\sqrt{1+[f_0'(x)]^2}}, \tag{8}$$

where $f'(x)$ is first derivative of $f_0(x)$. In order to calculate the total field $\psi(\boldsymbol{r}_0)$ at each point in the upper rough surface S_0 with consideration of the transmitted field, it is necessary to derive the value of scattering

coefficient in the approximation described below. In this section we derive the scattering coefficient in the KA as shown in Fig.2.

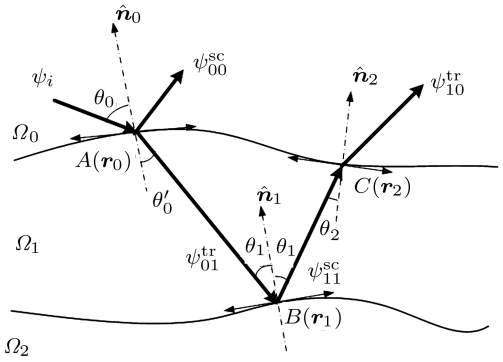


Fig.2. Configuration of the KA.

We assume that points in the upper and the lower rough surfaces each have a large radius of curvature relative to the wavelength of the incident fields. Under this assumption, the tangent plane hypothesis is valid and Fresnel laws can be locally used. Thus, at the point $A(\boldsymbol{r}_0)$ in surface S_0, we have

$$\psi_{00}^{\rm sc}(\boldsymbol{r}_0) = R_{01}(\boldsymbol{r}_0)\psi_i(\boldsymbol{r}_0), \tag{9a}$$

$$\frac{\partial\psi_{00}^{\rm sc}(\boldsymbol{r}_0)}{\partial n_0} = -R_{01}(\boldsymbol{r}_0)\frac{\partial\psi_i(\boldsymbol{r}_0)}{\partial n_0}, \tag{9b}$$

where $\psi_{00}^{\rm sc}(\boldsymbol{r}_0)$ is the field scattered in surface S_0 due to the incident field, and R_{01} is the Fresnel reflection coefficient, defined as

$$R_{ij}(\boldsymbol{r}) = \begin{cases} \dfrac{\cos\theta_k - (\varepsilon_j/\varepsilon_i - \sin^2\theta_k)^{1/2}}{\cos\theta_k + (\varepsilon_j/\varepsilon_i - \sin^2\theta_k)^{1/2}}, & \text{for horizontal polarization,} \\ \dfrac{\varepsilon_j/\varepsilon_i\cos\theta_k - (\varepsilon_j/\varepsilon_i - \sin^2\theta_k)^{1/2}}{\varepsilon_j/\varepsilon_i\cos\theta_k + (\varepsilon_j/\varepsilon_i - \sin^2\theta_k)^{1/2}}, & \text{for vertical polarization,} \end{cases} \tag{10}$$

where $\varepsilon_{i,j}$ is the relative permittivity of the medium $\Omega_{i,j}$ and $\theta_{k=0,1,2}$ represents the local incident angle as shown in Fig.2. Now, we consider the transmitted light. The field scattered into medium Ω_1 due to the incident field $\psi_i(\boldsymbol{r}_0)$ is given in surface S_0 by

$$\psi_{01}^{\rm tr}(\boldsymbol{r}_0) = T_{01}(\boldsymbol{r}_0)\psi_i(\boldsymbol{r}_0), \tag{11a}$$

$$\frac{\partial\psi_{01}^{\rm tr}(\boldsymbol{r}_0)}{\partial n_0} = T_{01}(\boldsymbol{r}_0)\frac{\partial\psi_i(\boldsymbol{r}_0)}{\partial n_0}, \tag{11b}$$

where $T_{ij} = \rho_{ij}(1 + R_{ij})$ is the Fresnel transmission coefficient. For the horizontal polarization $\rho_{ij} = 1$ and for the vertical polarization $\rho_{ij} = \sqrt{\varepsilon_i/\varepsilon_j}$. The transmitted beam from $A(\boldsymbol{r}_0)$ will intercept the lower interface at point $B(\boldsymbol{r}_1)$. It can be easily located by using the Fresnel law

$$\sin\theta_0' = \sin\theta_0\frac{1}{\sqrt{\varepsilon_1}}. \tag{12}$$

Then it is easy to obtain

$$\psi_{11}^{\rm sc}(\boldsymbol{r}_1) = R_{12}(\boldsymbol{r}_1)T_{01}(\boldsymbol{r}_0)\psi_i(\boldsymbol{r}_0)\mathrm{e}^{-jk\sqrt{\varepsilon_1}|\boldsymbol{r}_1-\boldsymbol{r}_0|}, \tag{13a}$$

$$\frac{\partial\psi_{11}^{\rm sc}(\boldsymbol{r}_1)}{\partial n_1} = -R_{12}(\boldsymbol{r}_1)T_{01}(\boldsymbol{r}_0)\frac{\partial\psi_i(\boldsymbol{r}_0)}{\partial n_0}\mathrm{e}^{-jk\sqrt{\varepsilon_1}|\boldsymbol{r}_2-\boldsymbol{r}_1|}, \tag{13b}$$

where k is the wave vector in medium Ω_0. Finally, the transmitted field $\psi_{10}^{\rm tr}(\boldsymbol{r}_2)$ at point $C(\boldsymbol{r}_2)$ can be written as

$$\psi_{10}^{\rm tr}(\boldsymbol{r}_2) = T_{10}(\boldsymbol{r}_2)R_{12}(\boldsymbol{r}_1)T_{01}(\boldsymbol{r}_0)\psi_i(\boldsymbol{r}_0)\mathrm{e}^{-jk\sqrt{\varepsilon_1}(|\boldsymbol{r}_2-\boldsymbol{r}_1|+|\boldsymbol{r}_1-\boldsymbol{r}_0|)}, \tag{14a}$$

$$\frac{\partial\psi_{10}^{\rm tr}(\boldsymbol{r}_2)}{\partial n_2} = T_{10}(\boldsymbol{r}_2)(-R_{12}(\boldsymbol{r}_1))T_{01}(\boldsymbol{r}_0)\frac{\partial\psi_i(\boldsymbol{r}_0)}{\partial n_0}\mathrm{e}^{-jk\sqrt{\varepsilon_1}(|\boldsymbol{r}_2-\boldsymbol{r}_1|+|\boldsymbol{r}_1-\boldsymbol{r}_0|)}. \tag{14b}$$

In order to obtain the transmitted field ψ_{10}^{tr} which means that the phase shift of the field between points $A(\boldsymbol{r}_0)$ and $C(\boldsymbol{r}_2)$ is to be calculated, it is necessary to determine numerically the locations of points $B(\boldsymbol{r}_1)$ and $C(\boldsymbol{r}_2)$. We do it as follows. Once the local incident angle θ of the transmitted beam is known (see Fig.3), it is easy to determine the projected point A' of $A(\boldsymbol{r}_0)$ in surface S_1 and we can find the two nearest points B_1' and B_2' with respect to point B' by searching the projected point of each point in the discrete surface S_1, which leads to finding the two nearest discrete points B_1 and B_2 with respect to point B in surface S_1. Finally, we obtain the numerical point B_{num} which is the crossing point of these two lines AB' and B_1B_2. Through the same process the numerical point C_{num} can be found. Then the phase shift $\Delta\varphi$ may be estimated by

$$\Delta\varphi = k\sqrt{\varepsilon_1}(AB_{\mathrm{num}} + B_{\mathrm{num}}C_{\mathrm{num}}). \tag{15}$$

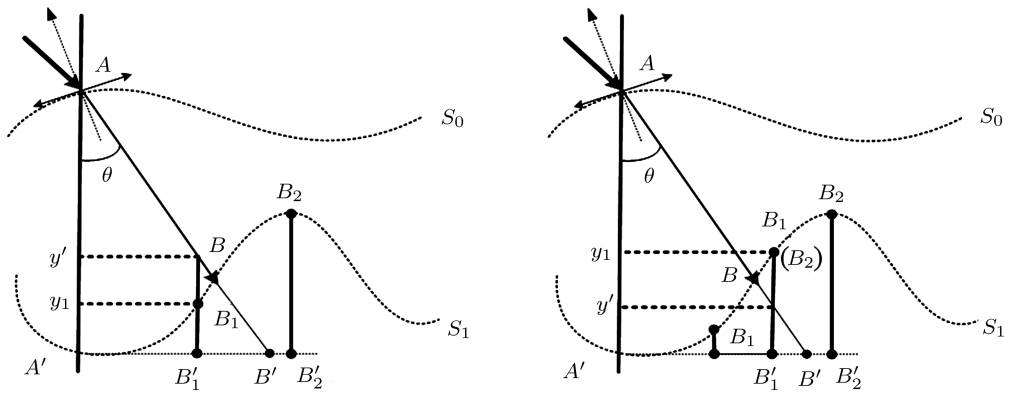


Fig.3. Scheme of the location of point.

Then $\psi_{10}^{\mathrm{tr}}(\boldsymbol{r}_2)$ is calculated by using Eq.(14). Finally we add at each point of S_0 the values $\psi_i(\boldsymbol{r})$, $\psi_{00}^{\mathrm{sc}}(\boldsymbol{r})$ and existent $\psi_{10}^{\mathrm{tr}}(\boldsymbol{r})$. Thus the total field at each point in surface S_0 (from Eqs.(9a), (9b) and (14)) is obtained as

$$\psi(\boldsymbol{r}_0) = \psi_i(\boldsymbol{r}_0) + \psi_{00}^{\mathrm{sc}}(\boldsymbol{r}_0) + \psi_{10}^{\mathrm{tr}}(\boldsymbol{r}_0)\,|_{\text{if exist}} = \psi_i(\boldsymbol{r}_0)\left[1 + R_{01} + T_{10}R_{12}T_{01}\mathrm{e}^{-j\Delta\varphi}\,|_{\text{if exist}}\right], \tag{16a}$$

$$\frac{\partial\psi(\boldsymbol{r}_0)}{\partial n_0} = \frac{\partial\psi_i(\boldsymbol{r}_0)}{\partial n_0} + \frac{\partial\psi_{00}^{\mathrm{sc}}(\boldsymbol{r}_0)}{\partial n_0} + \frac{\psi_{10}^{\mathrm{tr}}(\boldsymbol{r}_0)}{\partial n_0}\bigg|_{\text{if exist}} = \frac{\partial\psi_i(\boldsymbol{r}_0)}{\partial n_0}\left[1 - R_{01} - T_{10}R_{12}T_{01}\mathrm{e}^{-j\Delta\varphi}\,|_{\text{if exist}}\right]. \tag{16b}$$

To avoid artificial edge diffraction, the incident wave should not be expressed as a plane wave, instead it should contain a narrow-angle energy distribution, where the energy is distributed within the mean incident angle. The tapered plane wave developed by Thorsos[9] satisfies this requirement, and so it is chosen as the incident wave. Consider a tapered plane wave to be incident on the rough surface

$$\psi_i(\boldsymbol{r}) = \exp\left(-jk_0\left(x\sin\theta_i - z\cos\theta_i\right)\left(1 + w(\boldsymbol{r})\right)\right) \times \exp\left(-\left(\frac{x + z\tan\theta_i}{g}\right)^2\right), \tag{17}$$

where θ_i is the incident angle, g the tapering parameter, and $w(\boldsymbol{r})$ should be such a function that $\psi_i(\boldsymbol{r})$ obeys the wave equation to a higher order. Thus $w(\boldsymbol{r})$ is chosen to be

$$w(\boldsymbol{r}) = \frac{\left[2\left(\dfrac{x + y\tan\theta_i}{g}\right)^2 - 1\right]}{(kg\cos\theta_i)^2}, \tag{18}$$

Then it is easy to obtain

$$\begin{aligned}&\frac{\partial\psi_i(\boldsymbol{r}_0)}{\partial n_0}\\ &= (\nabla\psi_i(\boldsymbol{r}_0)\cdot\hat{\boldsymbol{n}}_0)\\ &= \psi_i(\boldsymbol{r}_0)\begin{bmatrix}-f_0(x_0)P_1 + \dfrac{2(x + f_0(x_0)\tan\theta_i)}{g^2}P_2\\ +P_3 + \dfrac{2\tan\theta_i(x + f_0(x_0)\tan\theta_i)}{g^2}P_2\end{bmatrix},\end{aligned} \tag{19}$$

where

$$P_1 = jk\sin\theta_i(1+w(\boldsymbol{r}_0)), \tag{20a}$$

$$P_2 = jk\frac{2(x_0\sin\theta_i - f_0(x_0)\cos\theta_i)}{(kg\cos\theta_i)^2} - 1, \tag{20b}$$

$$P_3 = -jk\cos\theta_i(1+w(\boldsymbol{r}_0)). \tag{20c}$$

Inserting Eqs.(17) and (19) into Eqs.(16a) and (16b), we can obtain the expressions of $\psi(\boldsymbol{r}_0)$ and $\dfrac{\partial\psi(\boldsymbol{r}_0)}{\partial n_0}$. With far-field restriction the following relationship then holds for the argument of the Green's function:

$$\begin{aligned} k\left|\boldsymbol{r}-\boldsymbol{r}_0\right| &= k(r^2 - 2\boldsymbol{r}_0\cdot\boldsymbol{r} + r_0^2)^{1/2} \\ &\sim kr\left[1 - \frac{\boldsymbol{r}_0\cdot\boldsymbol{r}}{r^2} + o\left(\frac{r_0}{r}\right)^2\right] \\ &\sim kr - k\hat{\boldsymbol{r}}\cdot\boldsymbol{r}_0, \end{aligned} \tag{21}$$

where $\hat{\boldsymbol{r}}$ is the unit vector in the $\boldsymbol{r}$ (observation) direction. The normal derivative of the Green's function is similarly evaluated by making the additional assumption that $k\left|\boldsymbol{r}-\boldsymbol{r}_0\right| \gg 1$, which is equivalent to $kr \gg 1$. Then the Green's function and its normal derivative, respectively, become

$$G(\boldsymbol{r},\boldsymbol{r}_0) \approx \sqrt{\frac{\mathrm{i}}{8\pi kr}}\exp(\mathrm{i}kr)\exp(-\mathrm{i}\boldsymbol{k}_s\cdot\boldsymbol{r}_0), \tag{22a}$$

$$\frac{\partial G(\boldsymbol{r},\boldsymbol{r}_0)}{\partial n_0} \approx \sqrt{\frac{\mathrm{i}}{8\pi kr}}\exp(\mathrm{i}kr)\exp(-\mathrm{i}\boldsymbol{k}_s\cdot\boldsymbol{r}_0)(-\mathrm{i}\boldsymbol{k}_s\cdot\hat{\boldsymbol{n}}_0). \tag{22b}$$

where $\boldsymbol{k}_s = k(\sin\theta_s\hat{\boldsymbol{x}} + \cos\theta_s\hat{\boldsymbol{z}})$ is scattering wave vector and θ_s is the scattered angle. Combining Eqs.(17), (19), (16), (22a), (22b) and Eq.(5), the scattered wave can be rewritten as

$$\psi_s(\boldsymbol{r}) = \sqrt{\frac{\mathrm{i}}{8\pi k_0 r}}\exp(\mathrm{i}kr)\psi_s^{(N)}(\theta_s), \tag{23}$$

where

$$\begin{aligned} \psi_s^{(N)}(\theta_s) = \int_{S_0}&\left[\psi(\boldsymbol{r}_0)(-\mathrm{i}\boldsymbol{k}_s\cdot\hat{\boldsymbol{n}}_0) - \frac{\partial\psi(\boldsymbol{r}_0)}{\partial n_0}\right] \\ &\times\exp(-\mathrm{i}\boldsymbol{k}_s\cdot\boldsymbol{r}_0)\mathrm{d}S_0 \end{aligned} \tag{24}$$

with $\mathrm{d}S_0 = \sqrt{1+[f_0'(x_0)]^2}\mathrm{d}x$. The bistatic scattering coefficient $\sigma(\theta_s)$ is determined as[12,13]

$$\sigma(\theta_s) = \frac{\left|\psi_s^{(N)}(\theta_s)\right|^2}{8\pi kg\sqrt{\dfrac{\pi}{2}}\cos\theta_i\left[1 - \dfrac{1+2\tan^2\theta_i}{2k^2g^2\cos^2\theta_i}\right]}. \tag{25}$$

Taking the shadowing effect into account and rectifying the bistatic scattering coefficient yield[7]

$$\sigma(\theta_s) = S(\theta_i,\theta_s)\sigma(\theta_s), \tag{26}$$

where $S(\theta_i,\theta_s)$ is the shadowing function

$$S(\theta_i,\theta_s) = \begin{cases} [1+\mathrm{erf}(v_s)](1-\mathrm{e}^{-2B_s})/(4B_s), & 0 \le \theta_s \le \theta_i, \\ [1+\mathrm{erf}(v_i)](1-\mathrm{e}^{-2B_i})/(4B_i), & \theta \le \theta_s \le \pi/2, \\ [\mathrm{erf}(v_i)+\mathrm{erf}(v_s)]\{1-\exp[-2(B_i+B_s)]\}/[4(B_i+B_s)], & \pi/2 \le \theta_s \le \pi, \end{cases} \tag{27}$$

with

$$B_{s(i)} = \left\{\exp(-9v_{s(i)}^2/8)/(3\pi v_{s(i)}^2)^{1/2} + \exp(-v_{s(i)}^2)/(\pi v_{s(i)}^2)^{1/2} - [1-\mathrm{erf}(v_{s(i)})]\right\}/4. \tag{28}$$

Here, $\mathrm{erf}(\cdot)$ is the error function and $v_{s(i)} = \left|\tan\theta_{s(i)}\right| l/\sqrt{2}\delta$.

4. Numerical results and discussions

In all the following numerical implementations, the relevant parameters of the Gaussian rough surface are measured in incident wavelength λ and the rough surface is created by 100 Monte Carlo realizations. The average height between the two interfaces is $d = 5\lambda$ for the scattering plots in Figs.4–7.

In order to examine the validity of the KA with consideration of the shadowing effects in this work, we first illustrate in Fig.4 the bistatic scattering coefficients of a single-layer Gaussian rough interface ($\varepsilon_1 = \varepsilon_2 = 1.6$) for different polarizations by using the classical MOM and the KA. The RMS height and the correlation length in the numerical implementation are set to be $\delta = 0.2\lambda$, and $l = 1.5\lambda$, respectively, which are in the KA assumption ($k_0 l > 6$, and $l^2 > 2.76\delta\lambda$). The incident angle θ_i is 40°, i.e. $\theta_i = 40°$. It is easily observed that the bistatic

scattering coefficient calculated in the KA with consideration of the tapered wave in our paper is in good agreement with that obtained by using the MOM over the most angular range, especially for the small and the moderate incident angles.

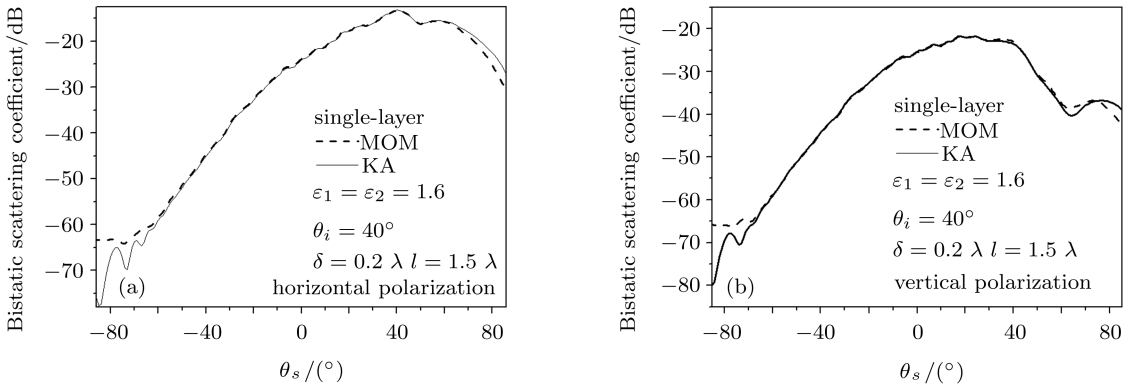


Fig.4. Bistatic scattering coefficients of a single-layer system with Gaussian rough interfaces by a tapered wave with different polarizations.

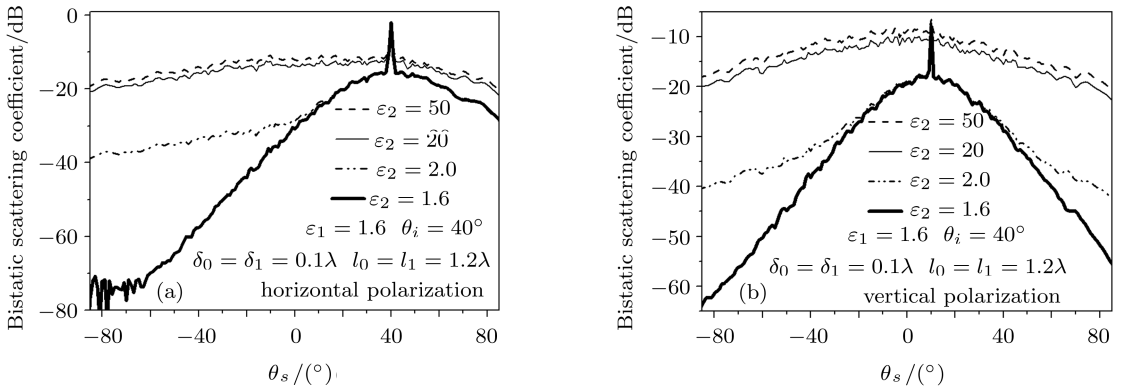


Fig.5. Bistatic scattering coefficients of the two-layer model versus ε_2 for different polarizations.

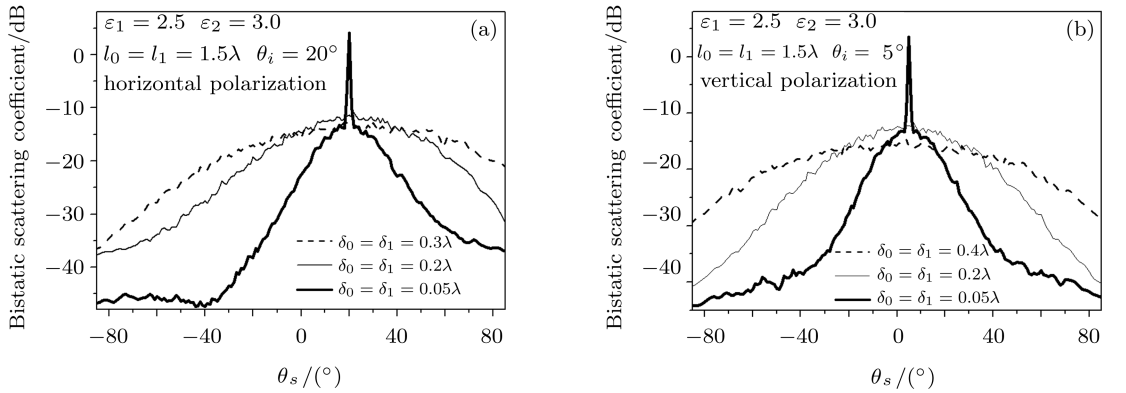


Fig.6. Bistatic scattering coefficients of the two-layer model versus the RMS height for different polarizations.

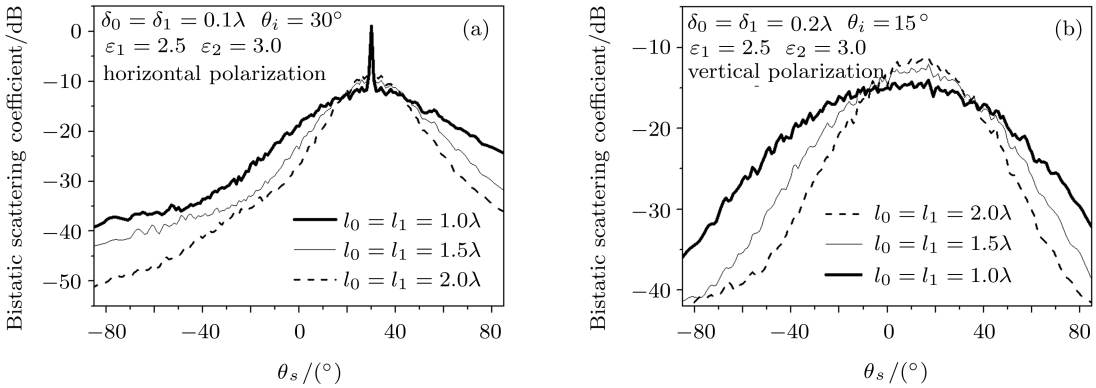


Fig.7. Bistatic scattering coefficients of the two-layer model versus l for different polarizations.

To further explore the important scattering characteristics of the two-layer Gaussian rough surface model, the dependence of the bistatic scattering coefficient on relative permittivity ε_2 is plotted in the KA for different polarizations in Fig.5 with incident angle $\theta_i = 40°$ for horizontal polarization (Fig.5(a)) and $\theta_i = 10°$ for vertical polarization (Fig.5(b)). The RMS heights of the upper rough surface and the lower rough surface are both 0.1λ and the correlative length is 1.2λ. It is found that the bistatic scattering coefficients of the layered model increases with the increase of ε_2 for different polarizations. It should be pointed out that for the case of $\varepsilon_2 = \varepsilon_1$, the two-layer media can be regarded as a single-layer medium, and the total scattered field in medium Ω_0 is just the scattered field $\psi_{00}^{\rm sc}(\boldsymbol{r}_0)$ in surface S_0 due to the incident field. As for the case of $\varepsilon_2 \neq \varepsilon_1$ that is concerned, the total scattered field in medium Ω_0 consists of $\psi_{00}^{\rm sc}(\boldsymbol{r}_0)$ in surface S_0 and $\psi_{10}^{\rm tr}(\boldsymbol{r})$ due to surface S_1, which leads the bistatic scattering coefficient of layered model to increase with the larger value of the relative permittivity ε_2 in the lower medium. Another point that is worth noting is that for the small value of ε_2, there is a more obvious peak in the specular direction for both polarizations. This phenomenon is caused mainly by the fact that the transmitted field increases with the large value of ε_2, which leads the incoherent scattering in the total scattering to increase, hence, the scattering peaks in the specular direction become small with the increase of ε_2.

In Fig.6, the effect of the RMS height on the bistatic scattering coefficient of the two-layer Gaussian rough surface with the same parameters (δ_0=δ_1, l_0=l_1) is also investigated, with incident angle $\theta_i = 20°$ for horizontal polarization (Fig.6(a)) and $\theta_i = 5°$ for vertical polarization (Fig.6(b)). The relative permittivities of media Ω_1 and Ω_2 are given by ε_1= 2.5 and ε_2= 3.0 respectively. The correlative lengths of surfaces S_0 and S_1 are both 1.5λ. It is observed that the bistatic scattering coefficients increase with RMS height for different polarizations over the most angular range except for in the specular direction. It is due mainly to the fact that the two-layer rough surface can be regarded as two flat interfaces for the small value of the RMS height, which results in the obvious peaks in the specular direction and weak incoherent scattering in the angular range far from the specular direction.

In Fig.7, the effects of the correlative length on the bistatic scattering coefficient of the two-layer Gaussian rough surface with the same parameters (δ_0=δ_1, l_0=l_1) are depicted. The incident angles θ_i are 30° for horizontal polarization (i.e. $\theta_i = 30°$ in Fig.7(a)) and 15° for vertical polarization (i.e. $\theta_i = 15°$ in Fig.7(b)) respectively. The relative permittivities of media Ω_1 and Ω_2 are the same as those in Fig.6. The RMS heights of surfaces S_0 and S_1 are both 0.1λ for Fig.6(a) and 0.2λ for Fig.6(b). It can be seen that the bistatic scattering coefficients increase with the decrease of the correlative length for different polarizations over the most angular range, the reason for this is that with the same RMS height, the smaller value of l means the larger value of the RMS slope coefficient of the two-layer rough surface, which results in the strong incoherent scattering (as shown by the

solid line in Fig.7). A comparison between the plots in Figs.7(a) and 7(b) shows that another point that is worth noting is that the values of the scattering peaks in the specular direction are dependent mainly on the value of the RMS height, in other words, the values of the scattering peaks are not sensitive to the variation in correlative length.

Figure 8 shows the scatterings from the two-layer system with different values of height d between the two interfaces for the horizontal polarization. The RMS height and the correlative length of the two-layered rough surface are 0.3λ and 1.5λ, respectively. The incident angle θ_i is 15° (i.e. $\theta_i = 15°$) and the relative permittivites of media Ω_1 and Ω_2 are the same as those in Fig.6. It is obvious that the bistatic scattering coefficient is almost not sensitive to the variation of the average height between the two interfaces.

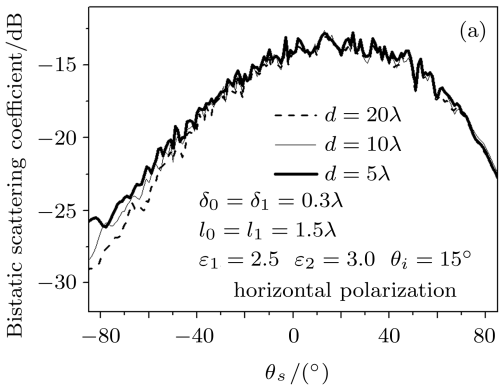


Fig.8. Bistatic scattering coefficients of the coefficients of the two-layer model with different values of roughness.

In Fig.9, the rough surface scatterings from two-layered Gaussian rough surface with different values of roughness are plotted for the horizontal polarization. The values of roughness for the upper rough surface are $\delta_0 = 0.2\lambda$ and $l_0 = 1.5\lambda$ for curves 1 and 2 and $\delta_0 = 0.3\lambda$ and $l_0 = 1.2\lambda$ for curves 3 and 4. The incident angle θ_i is 30° (i.e. $\theta_i = 30°$) and the relative permittivies of media Ω_1 and Ω_2 are also the same as those in Fig.6. It is shown that the bistatic scattering coefficient is more sensitive to the variation of the value of roughness for the upper rough surface (δ_0 and l_0) than that for the lower rough surface (δ_1 and l_1), which may be attributed to the fact that the value of field transmitted in medium Ω_0 is smaller than that of the field scattered in surface S_0 ($\psi_{00}^{\rm sc}(\boldsymbol{r}_0)$) due to the incident field.

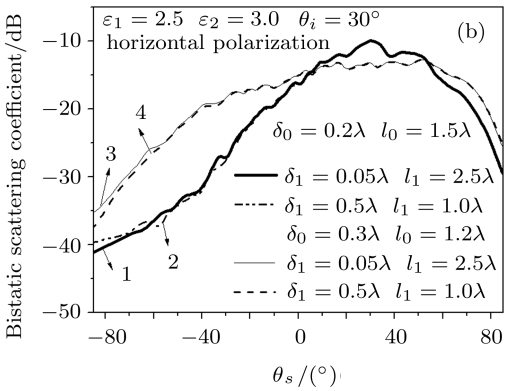


Fig.9. Bistatic scattering two-layer model with different values of d.

5. Conclusions

To investigate the bistatic scattering from the two-layer Gaussian rough surface, we use the KA with consideration of the shadowing effects to calculate the bistatic scattering coefficient of this two-layer system. The tapered incident wave is introduced into the KA and the bistatic scattering coefficient of KA is redetermined. The average field is computed by using the Monte-Carlo method for different polarizations. The bistatic scattering coefficient calculated in the KA with the introduction of the tapered wave in our paper is in good agreement with that obtained by using the MOM over the most angular range, which indicates the validity of the KA proposed in our paper. What remains in this respect is to calculate the scattering from two-layer lossy dielectric rough surface by using the method suggested in this paper, which is even more significant in engineering

References

[1] Wismann V, Gade M, Alpers W and Hühnerfuss H 1998 *Int. J. Remote Sens.* **19** 3607

[2] Blumberg D G, Freilikher V, Lyalko I, Wolfson L D, Kotlyar A L, Shevchenko V N and Ryabokonenko A D 2000 *IGARSS 2000, IEEE 2000 International* **5** 2011

[3] Jafari G R, Mahdavi S M, Iraji Zad A and Kaghazchi P

2005 *Surface and Interface Analysis* **37** 641
[4] Johnson B T, Shine K P and Forster P M 2004 *Quarterly Journal of the Royal Meteorological Society* **130** Part B 1407
[5] Murasaki T 2002 *Electronics and Communications in Japan* (Part II: *Electronics)* **85** 30
[6] Fuks I M and Voronovitch A 2000 *Waves in Random Media* **10** S253
[7] Ren Y C and Guo L X 2006 *Systems Engineering and Electronics* **28** 496
[8] Guo L X and Wu Z S 2000 *Acta Phys. Sin.* **49** 1065 (in Chinese)
[9] Thorsos E 1988 *J. Acoust. Soc. Am.* **83** 78
[10] Ogilvy J A 1991 *Theory of Wave Scattering from Random Rough Surface* (IOP Publishing in Bristol)
[11] Wang X, Wang C F and Gan Y B 2003 *Progress in Electromagnetics Research, PIER* **40** 207
[12] Qin L, Chan C and Tsang L 1999 *IEEE Trans. Antenna Propagat.* **47** 752
[13] Tsang L and Kong J A 2001 *Scattering of Electromagnetic Waves* (United States of America: John Wiley & Sons. Inc)